The EMBO Journal (2008) 27, 433–446 | © 2008 European Molecular Biology Organization | All Rights Reserved 0261-4189/08
www.embojournal.org

THE EMBO JOURNAL

Fission and selective fusion govern mitochondrial segregation and elimination by autophagy

Gilad Twig[1,6], Alvaro Elorza[1,6], Anthony JA Molina[1,2], Hibo Mohamed[1], Jakob D Wikstrom[1], Gil Walzer[1], Linsey Stiles[1], Sarah E Haigh[1], Steve Katz[1], Guy Las[1], Joseph Alroy[3], Min Wu[4], Bénédicte F Py[5], Junying Yuan[5], Jude T Deeney[2], Barbara E Corkey[2] and Orian S Shirihai[1,*]

[1]Department of Pharmacology and Experimental Therapeutics, Tufts University School of Medicine, Boston, MA, USA, [2]Obesity Research Center, Department of Medicine, Boston University School of Medicine, Boston, MA, USA, [3]Department of Pathology Tufts—NEMC and School of Veterinary Medicine, Boston, MA, USA, [4]Seahorse Bioscience, North Billerica, MA, USA and [5]Department of Cell Biology, Harvard Medical School, Boston, MA, USA

Accumulation of depolarized mitochondria within β-cells has been associated with oxidative damage and development of diabetes. To determine the source and fate of depolarized mitochondria, individual mitochondria were photolabeled and tracked through fusion and fission. Mitochondria were found to go through frequent cycles of fusion and fission in a 'kiss and run' pattern. Fission events often generated uneven daughter units: one daughter exhibited increased membrane potential ($\Delta\psi_m$) and a high probability of subsequent fusion, while the other had decreased membrane potential and a reduced probability for a fusion event. Together, this pattern generated a subpopulation of non-fusing mitochondria that were found to have reduced $\Delta\psi_m$ and decreased levels of the fusion protein OPA1. Inhibition of the fission machinery through DRP1^{K38A} or *FIS1* RNAi decreased mitochondrial autophagy and resulted in the accumulation of oxidized mitochondrial proteins, reduced respiration and impaired insulin secretion. Pulse chase and arrest of autophagy at the pre-proteolysis stage reveal that before autophagy mitochondria lose $\Delta\psi_m$ and OPA1, and that overexpression of OPA1 decreases mitochondrial autophagy. Together, these findings suggest that fission followed by selective fusion segregates dysfunctional mitochondria and permits their removal by autophagy.

The EMBO Journal (2008) **27,** 433–446. doi:10.1038/sj.emboj.7601963; Published online 17 January 2008
Subject Categories: membranes & transport; cellular metabolism
Keywords: autophagy; β-cell; fission; fusion; mitochondria

*Corresponding author. Department of Pharmacology and Experimental Therapeutics, Tufts University School of Medicine, 136 Harrison Avenue, Boston, MA, 02111, USA. Tel.: +1 617 230 8570; Fax: +1 617 636 6738; E-mail: orian.shirihai@tufts.edu
[6]These authors contributed equally to this work

Received: 9 March 2007; accepted: 20 November 2007; published online 17 January 2008

Introduction

Mitochondria in living cells form a dynamic reticulum that is continuously remodeled by fusion and fission events. Fusion generates networks with continuous membranes and matrix lumen. As a result, the constituents of each network share solutes, metabolites and proteins (Nakada *et al*, 2001; Arimura *et al*, 2004; Chen *et al*, 2005), as well as electrochemical gradient, making them electrically coupled (Skulachev, 2001; Twig *et al*, 2006). These characteristics of mitochondrial networks suggest that fusion is a mechanism by which intact mitochondria could complement a damaged unit and possibly recover its activity, thereby maintaining metabolic efficiency (Chan, 2006). However, recent reports question the role of fusion as a physiological mechanism for the recovery of depolarized mitochondria, since dissipation of mitochondrial membrane potential ($\Delta\psi_m$) using pharmacologic uncouplers resulted in extensive network fragmentation, degradation of the cellular Optic Atrophy-1 protein (OPA1, a fusion protein) and the inhibition of fusion (Legros *et al*, 2002; Meeusen *et al*, 2004; Duvezin-Caubet *et al*, 2006; Ishihara *et al*, 2006; Song *et al*, 2007). While pharmacologically induced collapse of cellular $\Delta\psi_m$ arrests fusion, it is yet unclear whether pairing of fusion mates is arbitrary or selective, and if depolarized mitochondria are indeed participating in the cycles of fusion and fission when surrounded by functional networks. Moreover, the event that generates a depolarized mitochondrion within the undisturbed cell is obscure if mitochondria exist in dynamic networks that permit diffusion and equilibration of matrix and membrane components. Thus, it is yet to be determined if networks are capable of giving rise to detached mitochondria that are functionally dissimilar from their source network. Addressing this question requires characterization of the consequences of the individual fission event.

While fusion may recruit dysfunctional mitochondria into the active pool, autophagy targets depolarized mitochondria for digestion and elimination (Elmore *et al*, 2001; Priault *et al*, 2005); the mechanism that sorts mitochondria between the two fates is still unclear (Levine and Yuan, 2005). If fusion and autophagy are competing fates of the depolarized mitochondria, we rationalize that fission might play a key role in allowing such competition to occur.

To determine if fusion/fission balance has a role in controlling the fate of a depolarized mitochondrion, proceeding to be rescued by complementation or to be eliminated by autophagy, it is necessary to determine if fission is essential for autophagy and if so, what mechanism triggers fission. Here we show that fusion triggers fission and that fission is essential for autophagy. Although the mitochondrial network appears to be homogenous, fission can produce metabolically different daughter units. Daughter mitochondria with reduced $\Delta\psi_m$ are less likely to re-fuse with the mitochondrial network and are more likely to be targeted by autophagy.

Results

Mitochondrial fusion is selective

We hypothesized that mitochondrial fusion is a selective process and tested the prediction that a subpopulation of mitochondria with low fusion capacity could be identified. Our goal was to follow these mitochondria and examine their metabolic function, source and fate. Fusion in INS1 cells was determined by the spread of mitochondrial matrix-targeted photoactivatable GFP (mtPA-GFP) from a subset of mitochondria throughout the mitochondrial network. In each cell, an area comprising approximately 10% of the cell cross-section area in a single focal plane was exposed to the two-photon laser stimulation, resulting in the labeling of 10–20% of the mitochondrial volume (square in Figure 1A). As a result of fusion, activated mtPA-GFP molecules spread to unlabeled mitochondria, resulting in a decrease in GFP fluorescence intensity (FI) of the mitochondria containing activated mtPA-GFP (Figure 1B; see 'Mitochondrial fusion assay' in the Supplementary data). Dilution of mtPA-GFP reached a steady state after 10–30 min. If mitochondria were non-selectively fusing with the network, we would expect to see a homogeneous distribution and dilution of the GFP signal. However, in 32% of the INS1 cells, a subpopulation of mitochondria failed to dilute their activated mtPA-GFP and carried the same GFP FI measured immediately after photoconversion ($n=22$). Similar results were obtained in primary mouse β-cells (60%, $n=10$; Figure 1D). The number of defined non-fusing mitochondrial structures detected in each cell was 3.1 ± 1.1. This represents the number of non-fusing mitochondria within the mitochondrial population that was labeled at the beginning of the experiment. (Therefore, if normalized per cell these would amount to ~20 mitochondria per cell.)

Compared with the average cellular $\Delta\psi_m$, determined by TMRE FI, the non-fusing mitochondria were depolarized. Quantitative analysis found a $26\%\pm5.3$ reduction in TMRE FI, equivalent to 7.8 ± 1.6 mV (Figure 1C; $P<0.001$, unpaired *t*-test).

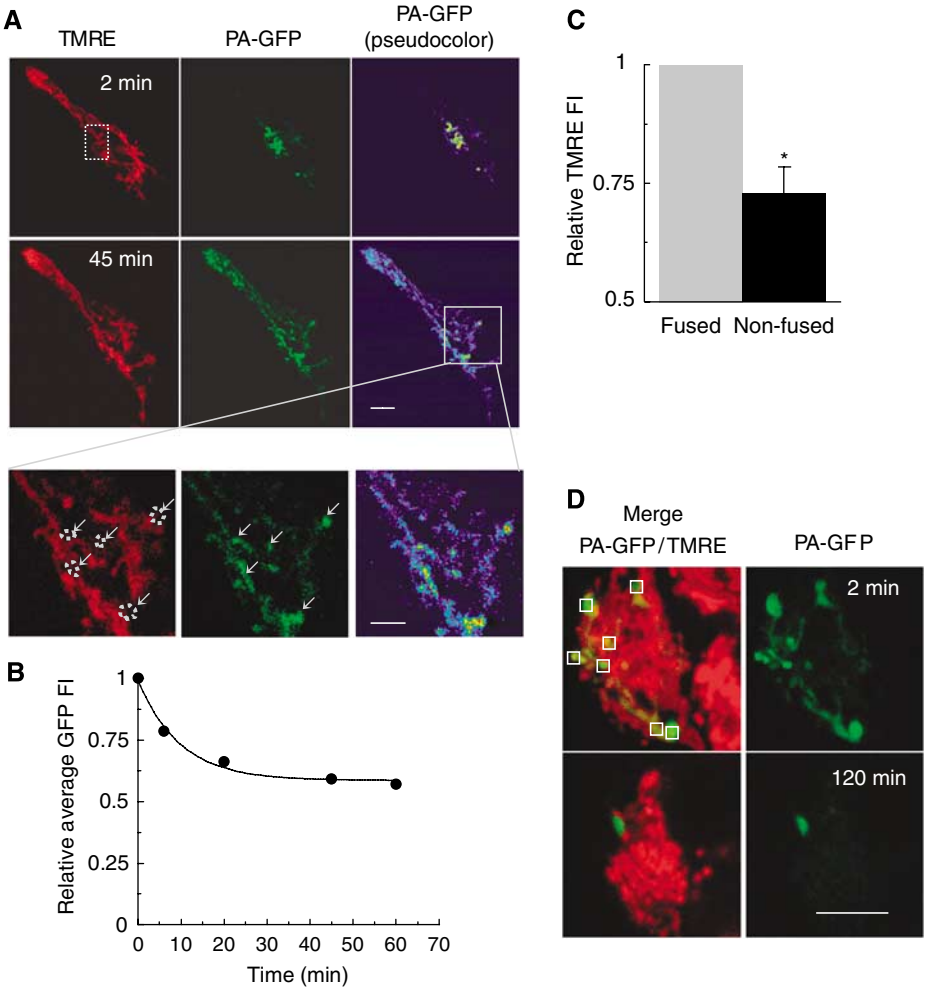

Figure 1 A subset of mitochondria have reduced fusion capacity. (**A**) INS1 cells were transduced with mtPA-GFP (green) and stained with TMRE (red). mtPA-GFP distribution is shown immediately (within 2 min) after photoactivation (area indicated by a dashed square) and in the plateau phase of mtPA-GFP spreading (45 min). Mitochondria that did not exhibit GFP FI decay (less than 5%) are marked by arrows. Upper scale bar, 10 μm; lower scale bar 5 μm. (**B**) Fusion events result in the spread of mtPA-GFP across the mitochondrial population, leading to its dilution and a decay in GFP FI value ($n=16$). (**C**) The relative difference in TMRE FI between non-fusing mitochondria and fusing mitochondria, calibrated against the whole-cell average. (**D**) Primary β-cells expressing mtPA-GFP were photoactivated in seven different regions (squares) and imaged after 2 min and again after 2 h of incubation. Scale bar, 10 μm. $^*P<0.001$.

Fusion and fission are paired consecutive events

To determine if segregation is upstream or downstream of depolarization, we characterized the life cycle of mitochondria in non-apoptotic INS1 and COS7 cells. Individual mitochondria were tagged and tracked with mtPA-GFP to temporally map fusion and fission events (Figure 2). Fusion and fission were paired and occurred most commonly as fusion quickly followed by fission (Figure 2A and B). Cumulative probability analysis indicates that fusion triggers fission, but fission has no effect on the timing of the following fusion (Figure 2C and D). In INS1 and COS7 cells we found that mitochondria spent the majority of their time in the post-fission, 'single state' (defined as the time interval from fission to fusion) and only 5.4–7.2% of the time in the post-fusion, 'fused state' (defined as the time interval between fusion and fission).

Membrane potential changes during fusion and fission

Double labeling of a single mitochondrion with mtPA-GFP and TMRE was used to determine the bioenergetic profile of the individual fission events (Figure 3A). Detailed description of measures taken in order to avoid imaging artifacts and laser-induced damage is provided in the Supplementary data. Changes in the ratio between TMRE and mtPA-GFP of the individual mitochondria were used to calculate deviations in $\Delta\psi_m$ as previously described (Twig *et al*, 2006). We found that during the intervals between pairs of fusion–fission events, $\Delta\psi_m$ of both INS1 and COS7 mitochondria was stable; spending 95% of the recording period within ± 2.7 mV of the average baseline (Figure 3C; Supplementary Figure S1). During fission, mtPA-GFP molecules redistributed and equilibrated between the two daughter mitochondria, and had GFP FI similar to the pre-fission mitochondrion ($\Delta_{\text{pre- and post-fission}} = 2.2 \pm 1.2\%$; $\Delta_{\text{daughters 1 and 2}} = 1.6 \pm 1.1\%$). Immediately after a fission event, however, large changes in $\Delta\psi_m$ were measured (Figure 3A–C). We observed the following patterns in 48 fission events:

(a) In 85% of fission events, one daughter mitochondrion depolarized (criterion = 2 mV) to a maximal amplitude of $+5.9 \pm 3.7$ mV, while the other daughter hyperpolarized (criterion = 2 mV) to a maximal amplitude of -6.5 ± 3.8 mV compared to pre-fission potential (Figure 3Bi). In 22% of these fission events, the

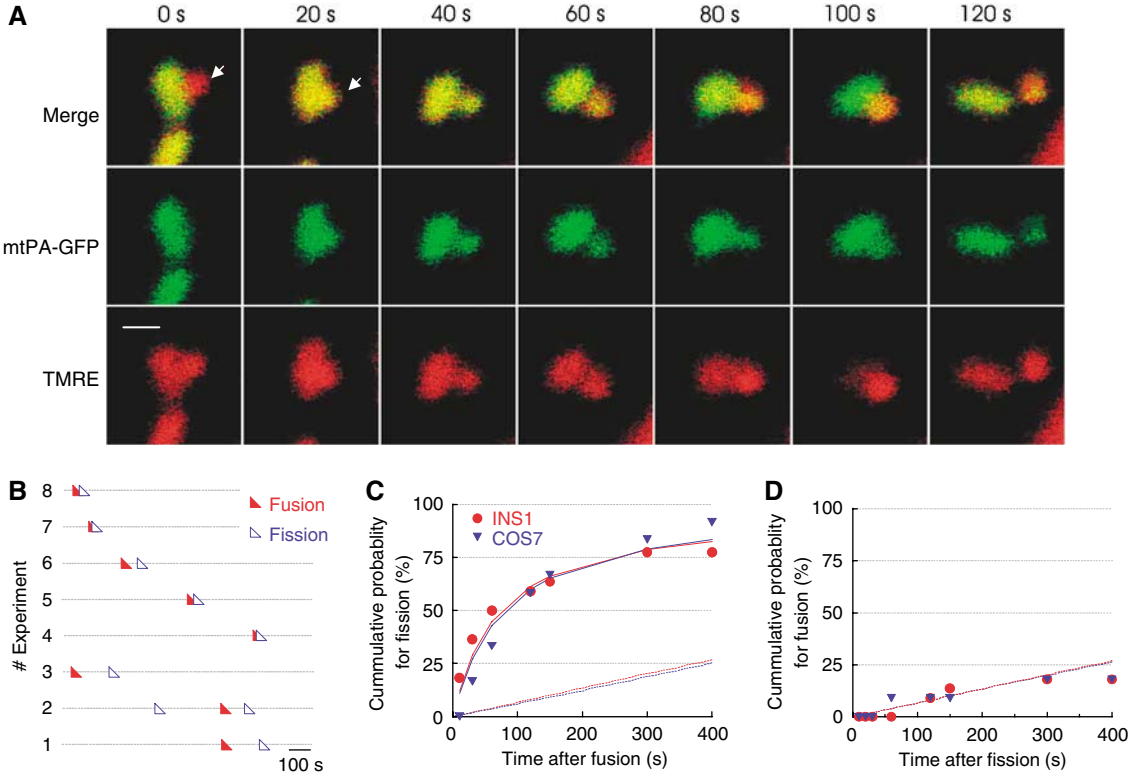

Figure 2 Tracking individual mitochondria over time reveals that fusion and fission are paired. (**A**) An INS1 cell expressing mtPA-GFP and co-labeled with TMRE. The two mitochondria fused 20 s after photoactivation (arrow in '20 s'). Then, a voltage difference was established between the two poles (60–120 s) and they were later physically separated (120 s). The pattern is qualitatively similar to that shown in Figure 3Bi. Scale bar, 2 μm. (**B**) Fusion and fission time chart for individual mitochondria. Individual mitochondria tagged with mtPA-GFP were monitored for a period of 1 h and the occurrence of fusion and fission was recorded. Mitochondria in INS1 and COS7 cells spend 77 s ($\pm$71 s) and 87 s ($\pm$78 s), respectively, in the post-fusion, connected state, and an average of 1434 s and 1172 s, respectively, in the solitary, post-fission state. (**C**) Fusion triggers fission. Cumulative probability of the occurrence of fission events at different intervals after fusion events occur (fraction of all fission events occurring after the given time interval). The data are fit to a hyperbolic function representing linkage between the two events (INS1, $R^2 = 0.98$; COS7, $R^2 = 0.96$). The straight line shows the predicted linear growth rate in fission event probability over time that would be expected if the fission had occurred independently from the fusion events (dashed lines INS1, $R^2 = 0.77$; COS7, $R^2 = 0.84$; see Supplementary data). (**D**) Fission does not trigger fusion. Cumulative probability of the occurrence of fusion events at different intervals after the fission event occurred. The data points were fitted to a linear relationship ($R^2 = 0.92$), as predicted if fusion occurred independently of fission (0.05 versus 0.06%/second, respectively; see Supplementary data).

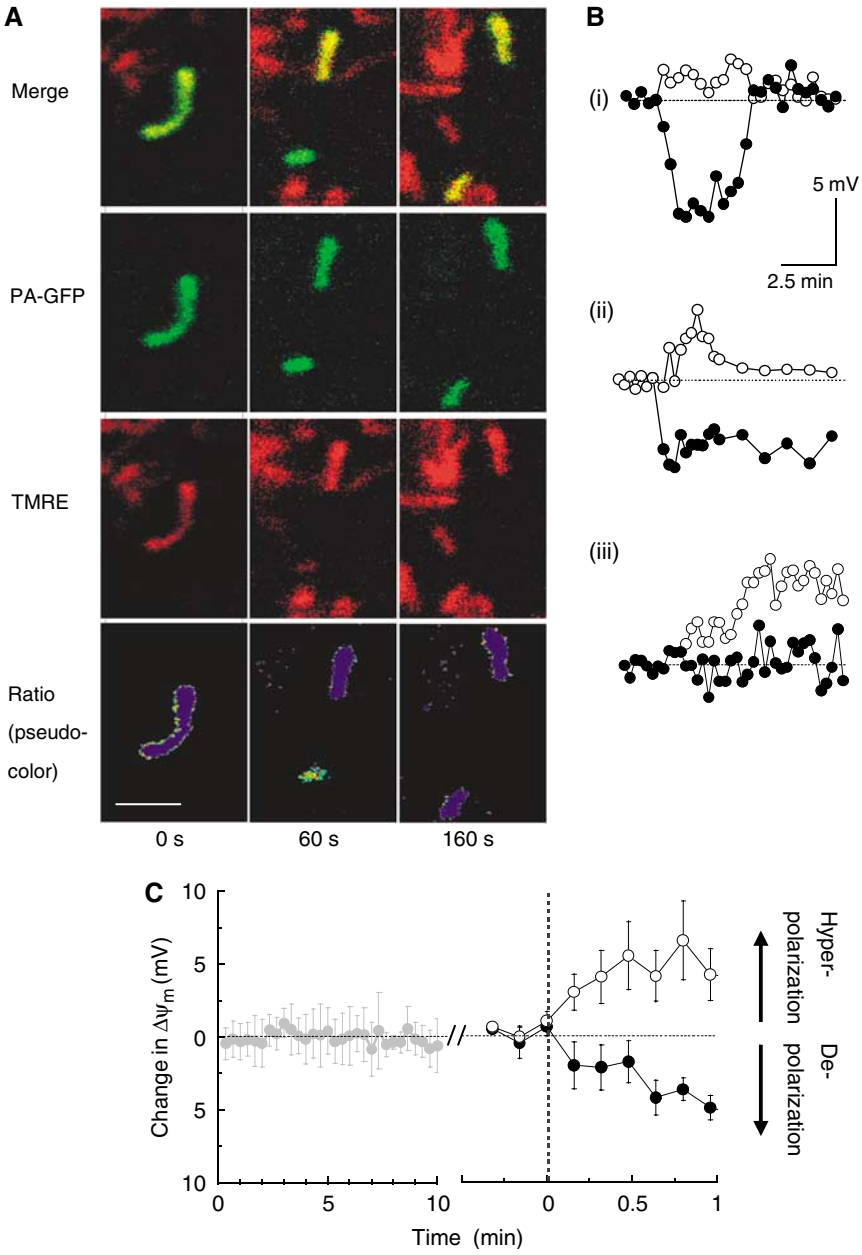

Figure 3 Metabolic outcomes of single fission events. (**A**) Mitochondrial fission in a COS7 cell yields two daughter mitochondria with a ~28% difference in TMRE/GFP FI ratio (~$\Delta = 9$ mV). The relative GFP FI change was minimal ($\Delta = 3.4\%$). For clarity the pseudocolored ratios before fission at 60 and 160 s after fission are shown. Scale bar, 2 μm. (**B**) Chart of $\Delta\psi_m$ over time for typical fission events; (i) fission results in temporary depolarization of one unit, (ii) fission results in permanent depolarization of one unit, (iii) fission results in the generation of a hyperpolarized daughter mitochondrion and a mitochondrion of the pre-fission potential. (**C**) Average $\Delta\psi_m$ before (left, gray) and after fission (right, filled and empty circles denote depolarized and hyperpolarized mitochondria respectively). Only fission events where $\Delta\psi_m$ of both mitochondria could be continuously tracked are included ($n = 7$).

post-fission depolarization phase was sustained without recovery (Figure 3Bii). The depolarized units were followed for additional 10–30 min. Fisher's one-sided probability analysis indicates that this pattern (Figure 3Bii) of $\Delta\psi_m$ change did not occur preferentially in *de novo* fission events as compared with those that followed fusion events ($P = 0.34$).

(b) In 4% of fission events, one daughter had similar $\Delta\psi_m$ as before fission while the other daughter hyperpolarized (Figure 3Biii). In these cases, the mother mitochondrion was relatively depolarized by 7–10 mV relative to the average cellular $\Delta\psi_m$. These patterns were significantly associated with *de novo* fission, not preceded by fusion (two-sided, $P = 0.049$).

(c) In 11% of fission events, both daughters had no change in $\Delta\psi_m$.

Potential mechanisms for the observed depolarization were tested and ruled out:

(a) Generation of a pore during fission; no leakage of mtPA-GFP was observed;

(b) Increase in ATP synthase activity; depolarization was observed with 1 μM oligomycin, $n=4$;
(c) Reduced fuel availability or Krebs cycle function; depolarization was observed in the presence of methyl succinate, a membrane-permeable fuel, $n=3$;
(d) Opening of the permeability transition pore; depolarization was observed with 1 μM cyclosporin A, $n=4$;
(e) Translocation of mitochondrion (from perinuclear to subplasmalemmal and vice versa; see Supplementary data);
(f) Engulfment of the daughter mitochondrion by an autophagosome (AP); autophagy occurs hours after depolarization and depolarized mitochondria are more frequent when autophagy is inhibited (Supplementary Figure S4; Figure 7E).

Depolarized daughter mitochondrion is unlikely to fuse

To test whether fission-induced changes in $\Delta\psi_m$ orchestrate subsequent fusion events, we followed the depolarized and the hyperpolarized daughters and recorded subsequent fusion events (Figure 4). The probability that a hyperpolarized daughter mitochondrion would fuse within 3 min post-fission was six times higher than that of a depolarized daughter mitochondrion, with a mean time interval of 105 s between fission and fusion (range 40–620 s; $n=8$). Representative schematic illustrations of these events are shown in Figure 4A. Fisher's two-sided probability analysis indicates that the depolarized daughter mitochondrion has a significantly lower probability of undergoing a fusion within 150 s after fission ($P=0.03$). In two experiments, depolarized mitochondria with $\Delta\psi_m$ 9–10 mV below the cell $\Delta\psi_m$ average were observed to undergo fission and generate a hyperpolarized daughter that went through subsequent fusion (data not shown).

$\Delta\psi_m$ Depolarization occurs hours before autophagy

It has previously been suggested that metabolically impaired mitochondria are preferably targeted by autophagy (Elmore *et al*, 2001; Priault *et al*, 2005). The time interval between depolarization and autophagy would indicate whether the isolation membrane of the early AP contributes to the segregation of depolarized daughter mitochondria and to their reduced fusion probability. Mitochondria, lysosomes, APs and autophagolysosomes (late APs) were imaged in the presence and absence of proteolytic enzyme inhibitors, E64d and pepstatin A. We found that unless digestion of late APs content is pharmacologically arrested, colocalization of mitochondria with AP markers is rarely captured (Supplementary Figure S2). Inhibition of proteolysis in late APs results in the accumulation of 15–30 APs within 30 min, indicating a high turnover rate of APs and fast removal of mitochondria after autophagy has started (Supplementary Figure S2).

To reveal whether mitochondria depolarize before or after the onset of autophagy, we determined the $\Delta\psi_m$ of autophagocytosed mitochondria at different time points before autophagy (Figure 4B; Supplementary Figure S10). $\Delta\psi_m$ was determined by pulsing the cells with $\Delta\psi_m$-dependent dye, mitotracker red (MTR), at different time points. Mitochondria that were pulse labeled 24 h before detection of autophagy had bright MTR staining, indicative of intact $\Delta\psi_m$ during the staining period (Figure 4B and C). However, those pulsed 1–3 h before detection of autophagy had dim MTR staining, indicating that depolarization occurred one or more hours before their engulfment. To ascertain that MTR itself does not induce or inhibit autophagy, the effect of MTR on the conversion of LC3-I to LC3-II, a marker for the activation of autophagy, was tested in INS1 cells treated with MTR for 24 h. MTR at the concentrations used for the above experiment had no effect on autophagy (data not shown). To verify that the observed aggregates of LC3:GFP are formed by APs and do not represent an expression artifact, LC3:GFP expressing cells were treated with the autophagy inhibitor 3-MA and aggregates were quantified. No aggregates were observed under these conditions.

This sequence of events was also supported by the following observations: (a) after 50 min of tracking individual mitochondria with reduced $\Delta\psi_m$, there was no reduction in mtPA-GFP intensity as would be expected if these units were consumed and digested (Supplementary Figure S3), and (b) inhibition of autophagy does not result in the recovery of depolarized mitochondria but rather in their accumulation as observed in INS1 (Figure 7E, $n=6$), MEF (Supplementary Figure S4C, $n=10$) or rat liver H4 (Supplementary Figure S4A, $n=5$). Together, these results indicate that reduced fusion capacity of the depolarized daughter is unlikely due to engulfment by APs.

Reduced OPA1 characterizes non-fusing and autophagocytosed mitochondria

The long time gap between depolarization and autophagy suggested that mitochondria spend a long period of time as non-fusing mitochondria prior to autophagy. It was therefore hypothesized that before autophagy mitochondria lose their fusion capacity potentially by degradation of a fusion protein such as OPA1. To test this hypothesis, we performed an immunoreactivity study of non-fusing mitochondria (Figure 5A) and of mitochondria inside APs (Figure 5B). To determine the protein level of OPA1 in non-fusing mitochondria, cells expressing mtPA-GFP and mtDsRed were subjected to fusion assays as described in Figure 1A. Two hours after photoconversion, cells were fixed, permeabilized and immunostained using a monoclonal antibody to the C-terminus of OPA1 (amino acids 708–830 in hOPA1; Alavi *et al*, 2007). Non-fusing mitochondria were identified as those that did not equilibrate their photoconverted mtPA-GFP with the unlabeled mitochondria over a period of 2–3 h, so that their GFP FI was over two folds higher as compared with the average mitochondria in the same cell. The ratio of OPA1 to mtDsRed was determined and was reduced in mitochondria that maintained high intensity of mtPA-GFP (Figure 5A), indicating that non-fusing mitochondria are characterized by reduced OPA1 immunoreactivity. Next, we determined OPA1 immunoreactivity in mitochondria inside APs (Figure 5B). Proteolytic activity was inhibited for 2–4 h using pepstatin A and E64d in cells expressing LC3:GFP and the matrix protein mtDsRed, both introduced by lentiviral transduction. The efficiency of the antiproteolytic activity was verified by the intact fluorescence of both the matrix protein mtDsRed and LC3:GFP. As compared with mitochondria outside APs, those inside had significantly reduced OPA1 immunoreactivity ($P=0.003$), but unchanged mtDsRed FI ($P=0.38$). To control for a potential artifact that might arise from partial proteolytic activity, we repeated this experiment this time inhibiting lysosomal

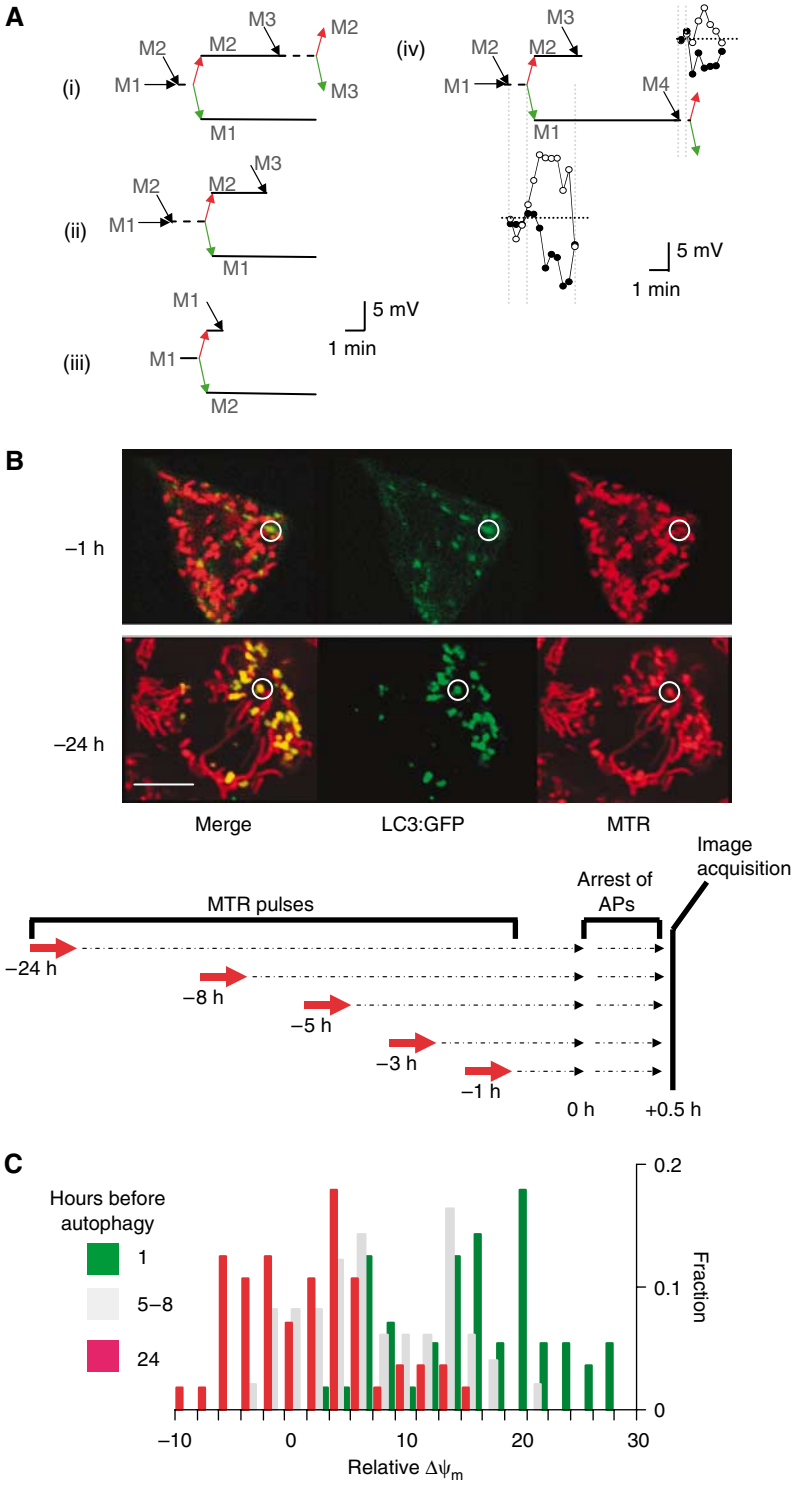

Figure 4 Consequences of fusion–fission events. (**A**) Schematic illustrations of mitochondrial tracking in four different experiments (i–iv) and corresponding $\Delta\psi_m$ traces (iv). Colored arrows indicate generation of hyperpolarizing (red) and depolarizing (green) daughters during fission. Note that after a fission event, fusion (black arrows) preferably occurred in the hyperpolarized daughter mitochondrion. (**B**) Depolarized mitochondria are selectively targeted for autophagy after a multi-hour time lag. APs are labeled with LC3:GFP, which translocates from the cytosol to the AP's isolation membrane. MTR, a membrane potential dye that stains mitochondria irreversibly and is retained during depolarization, is used to pulse label mitochondria in INS1 cells (14 min, 50 nM) at different time points before detection of APs content. At the time set for detection, cells were treated with pepstatin A (10 μM) and E64d (10 μM) for 30 min to arrest digestion inside the APs, and then subjected to confocal microscopy (see schematic illustration of the Materials and methods). MTR pulse is used here to report on $\Delta\psi_m$ during the staining period. While mitochondria outside APs show bright MTR fluorescence, those localized in APs varied in fluorescence based on the time at which they were pulsed with MTR. Note that mitochondria inside APs have dim MTR FI if they were pulsed with MTR 1 h before autophagy was detected (circle, top panel), but bright MTR FI if pulsed 24 h before detection of autophagy (circle, bottom panel). Scale bar, 10 μm. (**C**) Distribution of MTR FI (given in $\Delta\psi_m$) of AP-localized mitochondria at different times before autophagy. Values are relative to cell's average MTR FI. In the *x*-axis, a zero value represents the average $\Delta\psi_m$ and positive values represent depolarized mitochondria.

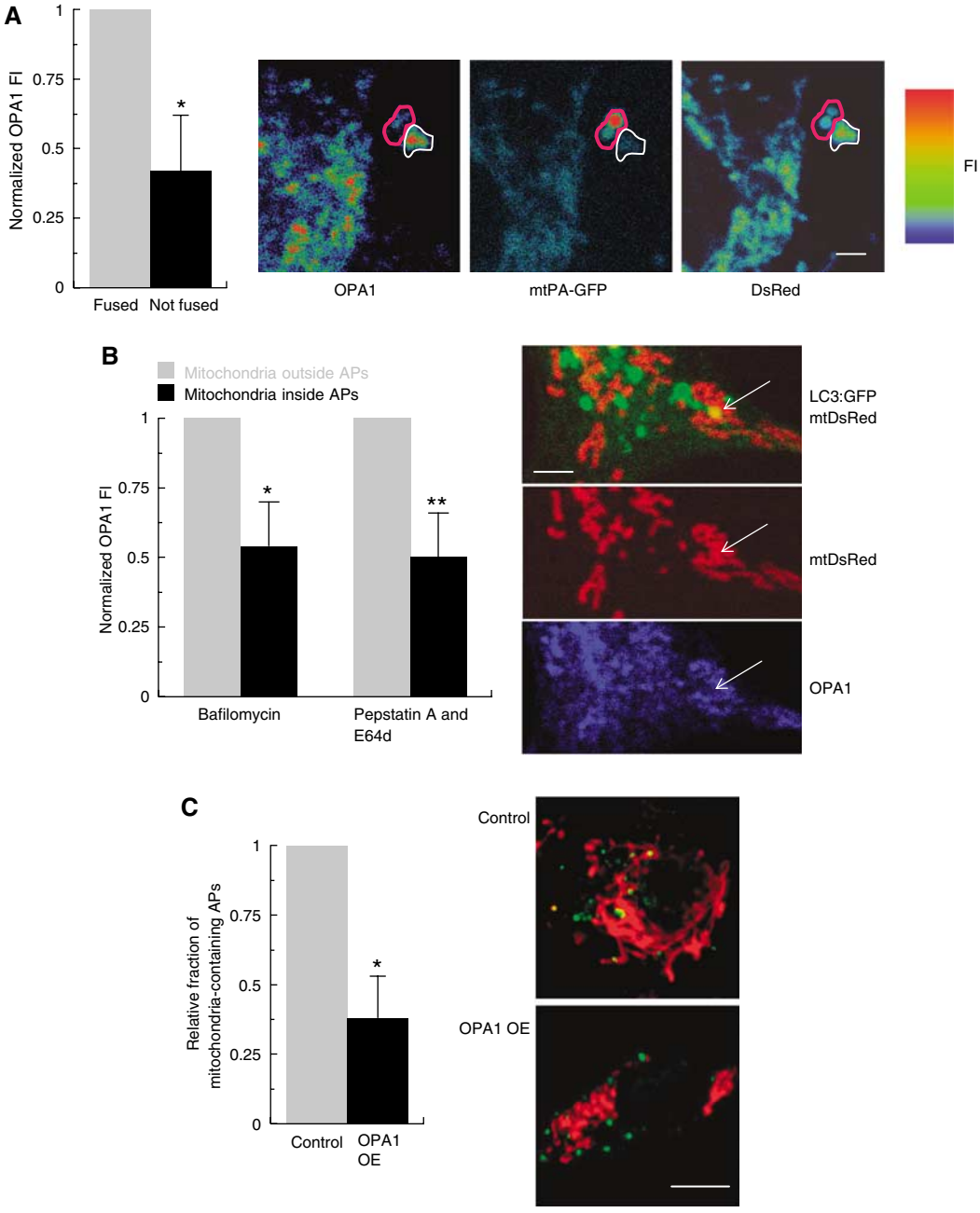

Figure 5 Reduced OPA1 levels in non-fusing mitochondria and mitochondria inside APs. (**A**) Relative immunofluorescence of OPA1 in INS1 cell mitochondria correlates to their fusion capacity. Cells ($n=6$) were photoactivated (~10–15% of cell mitochondrial mass) and then returned to the incubator for 2 h before fixation. Based on their ability to share and thereby dilute the photoconverted mtPA-GFP, mitochondria were classified as fused ($n=54$) in which GFP FI was lower than 2 times the average and non-fused ($n=10$) in which GFP FI was at least 200% above the average (in the same manner as described for Figure 1). In each cell, OPA1 FI of non-fused mitochondria was normalized to that of mitochondria that had diluted mtPA-GFP through fusion. OPA1 FI is reduced in non-fusing mitochondria ($P=0.003$). A set of FI-coded images of mtPA-GFP, mtDsRed and OPA1 immunostaining are shown. Scale bar, 2 μm. (**B**) OPA1 FI, but not mtDsRed FI, is reduced in mitochondria undergoing autophagy. INS1 cells expressing mtDsRed and LC3:GFP were treated with 0.2 μM bafilomycin (45 min) or a cocktail of pepstatin A and E64d (90 min) and fixed. Mitochondria inside APs were defined by colocalization of mtDsRed and LC3:GFP. OPA1 FI in APs was normalized to its FI in mitochondria that were located outside APs (organelles positive for mtDsRed with subthreshold GFP FI). OPA1 FI within APs was 50% (*$P<0.001$) and 54% (**$P=0.003$) upon treatment with bafilomycin or a cocktail of pepstatin A and E64d, respectively. Mitochondria inside APs had similar (96%) mtDsRed FI to those located outside APs ($P=0.47$). Scale bar, 2 μm. (**C**) The effect of OPA1 overexpression on the number of AP-containing mitochondria. Imaging of INS1 cells already expressing LC3:GFP and mtDsRed was performed 48–72 h after adenoviral transduction with either OPA1 overexpression or control (mitoPA-GFP). The number of AP-containing mitochondria in the OPA1 overexpression (OE, $n=6$) was normalized to the control (*$P=0.001$). Images show representative cells from each group. Red, mtDsRed; green, LC3:GFP. In the control cell, note the colocalization of APs with mitochondria. Scale bar, 10 μm.

V-ATPase with bafilomycin, which inhibits the fusion of lysosome with the early AP and preserves the mitochondrial morphology inside the AP (for electron microscopy of bafilomycin-treated APs, see Supplementary Figure S8). Similar reduction in OPA1 immunoreactivity was observed under these conditions ($P<0.001$; Figure 5B).

To determine if the observed reduction in OPA1 contributed to the targeting of mitochondria to AP, OPA1 was overexpressed by transduction with adenoviruses in INS1 cells stably expressing LC3:GFP and mtDsRed. Mitophagy (mitochondrial autophagy) was determined by counting mitochondria-containing APs under conditions in which proteolysis inside the APs was pharmacologically arrested for 1 h. Mitophagy was found to be reduced by 64% in OPA1-overexpressing cells as compared with control cells transduced with mtPA-GFP adenovirus (Figure 5C, $P<0.001$). Total number of APs was not significantly different (APs per cell: control, 47.4 ± 19; OPA1 OE, 35.1 ± 21). As previously reported, OPA1 overexpression can result in either a decrease or an increase in mitochondrial size (Cipolat *et al*, 2004; Griparic *et al*, 2004; Chen *et al*, 2005). Similar to MEF cells, OPA1 overexpression in INS1 cells resulted in a general but relatively homogenous reduction in mitochondrial size, while mitochondrial fusion activity remained intact (Chen *et al*, 2005). These observations rule out that decreased autophagy was solely due to increased mitochondrial size.

Inhibition of fission reduces mitochondrial autophagy

The reciprocal dependence of fusion and autophagy on $\Delta\psi_m$ suggests that mitochondrial fission may play a key role in segregating and uncoupling mitochondria from the network, thereby enabling depolarization and autophagy of dysfunctional daughter units. The role of fission in mitochondrial autophagy was evaluated in INS1 cells expressing low levels of FIS1, the rate-limiting protein in the mitochondrial fission process (Yoon *et al*, 2003; Okamoto and Shaw, 2005) and in cells expressing a dominant-negative form of the fission protein DRP1 ($DRP1^{K38A}$, or DRP1-DN). Both were introduced by lentiviral transduction and tested within 10 days of the infection (see Supplementary Figure S5A and B; Stojanovski *et al*, 2004). Expression of DRP1-DN resulted in the transformation of mitochondrial architecture to the characteristic elongated tubules with enlarged circular ends (Figure 7B; Supplementary Figure S9). The effect of *FIS1* RNAi on mitochondrial morphology is milder and was verified by morphometric analysis (Supplementary Figure S5C). Inhibition of mitochondrial fission resulted in reduction of the number of mitochondria-containing

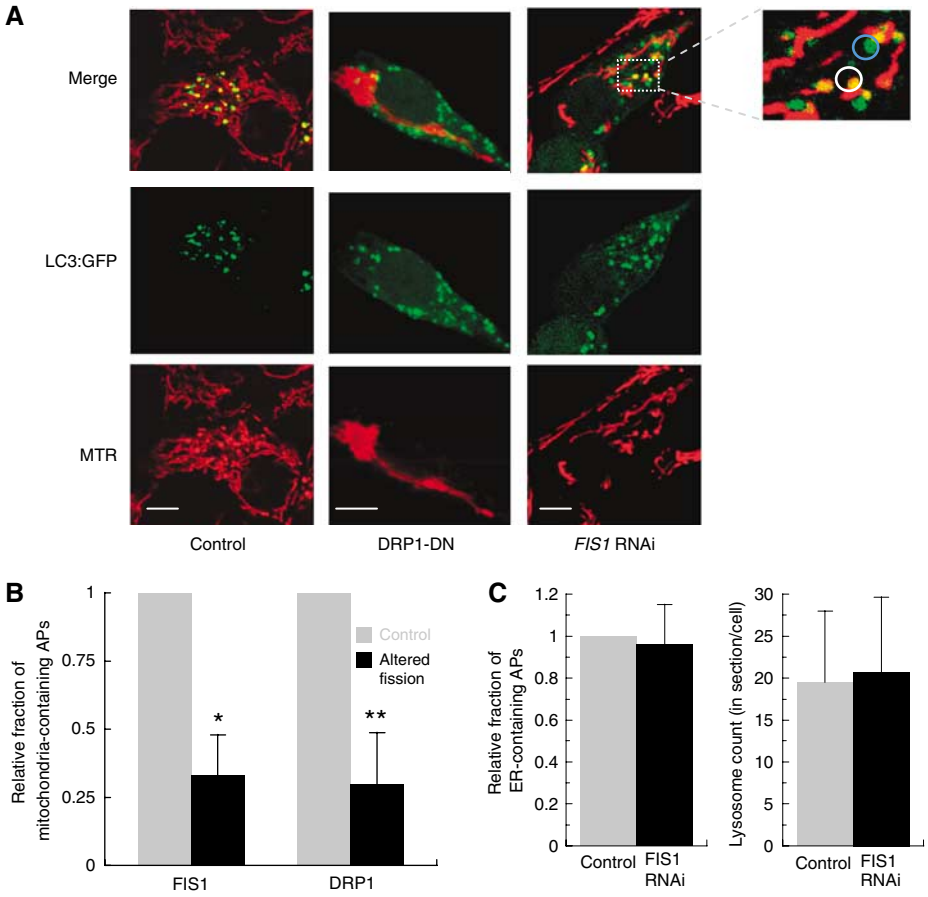

Figure 6 Inhibition of fission attenuates mitochondria-specific autophagy (mitophagy). (**A**) Confocal images of *FIS1* RNAi, DRP1-DN and control cells coexpressing the AP marker LC3:GFP (green), and stained with MTR (red, control and *FIS1* RNAi group) or mtDsRed (red, DRP1-DN) and treated with pepstatin A and E64d to arrest digestion in late APs. A magnified area within a *FIS1* RNAi cell shows APs with and without mitochondria (white and blue circles respectively). Scale bar, 5 μm. (**B**) Quantitative analysis of AP-containing mitochondria in INS1 cells expressing *FIS1* RNAi or DRP1-DN. In each group the number of AP-containing mitochondria was normalized to its control and found to be significantly different (*$P<0.001$; **$P<0.001$). (**C**) Altering fission does not impair ER autophagy and AP or lysosomal mass. INS1 cells expressing LC3:GFP were stained with ER Tracker to assess AP-containing ER. The number of AP-containing ER was not significantly different between control and *FIS1* RNAi cells ($P=0.51$; $n=11$). Lysosensor stain (75 nM, 30 min) reveals no difference between control and *FIS1* RNAi cells ($P=0.21$). The total AP number in DRP1-DN cells is similar to that of the control ($n=11$, $P=0.53$).

APs ($P<0.001$; Figure 6A and B) but not in the number of ER-containing APs (*FIS1* RNAi group, $P=0.51$; Figure 6C). The total number of lysosomes (Figure 6C) and the total number of APs remained without a significant change (DRP1-DN group: $n=11$, $P=0.53$; *FIS1* RNAi group: $n=12$, $P=0.59$).

While mitochondrial autophagy was inhibited, the assembly of the isolation membrane and the propagation of the AP to late AP was not affected by *FIS1* RNAi, as indicated by (a) unchanged maximal AP formation capacity detected by long-term exposure to E64d and pepstatin A (control 24 ± 5, *FIS1* RNAi 21 ± 7), (b) resumption of AP digestion in <1 min after E64d and pepstatin A were removed from the media (data not shown), (c) no difference in lysosome formation capacity between the control and the *FIS1* RNAi groups as indicated by counting lysosomes stained with lysosensor blue dye (Figure 6C; Supplementary Figure S6) and (d) electron micrographs showing normal appearance of early and late APs as obtained by treatment with the protease inhibitors pepstatin A and E64d, or with the lysosomal V-ATPase inhibitor bafilomycin (Supplementary Figure S8).

Fission-deficient mitochondria have more oxidized protein but less ROS

We hypothesized that inhibition of fission would reduce segregation and degradation of dysfunctional mitochondria and thus result in accumulation of damaged mitochondrial proteins. Levels of mitochondrial protein oxidation in cells expressing *FIS1* RNAi were 1.7-fold higher than in control RNAi (Figure 7A, $n=4$). Similar effect was found in DRP1-DN-treated cells where both carbonylated protein and nitrotyrosine were accumulated (Figure 7A and B). To test the possibility that the latter finding arose from overproduction of ROS in *FIS1* RNAi cells, ROS generation was assessed using dihydroethidium (DHE) (Figure 7C). There was an insignificant decrease in ROS production in cells expressing *FIS1* RNAi compared with control RNAi under normal culture conditions (11 mM glucose; $P=0.50$). This decrease became significant using 22 mM glucose ($P<0.001$). These results suggest that the observed increase in oxidized protein in fission-deficient cells is the result of accumulation rather than excess generation of damage. To test if inhibition of autophagy affects the accumulation of oxidized proteins in mitochondria, we inhibited fusion between lysosomes and APs with bafilomycin A1 (0.1 μM) and determined carbonylated proteins (Figure 7D). Treatment with bafilomycin A1 for as short as 3 h resulted in increased levels of oxidized proteins in mitochondria and in the accumulation of early APs as revealed by increased LC3-II band. Treatment with 3-MA (2 mM, 5 days), which inhibits the initiation of the early AP, resulted in increased subcellular heterogeneity in $\Delta\psi_m$ and the appearance of small depolarized mitochondria (Figure 7E). A similar effect was observed in two autophagy deficient cell lines, Beclin1 RNAi H4 and ATG5−/− MEF cells (Supplementary Figure S4A and C).

FIS1 knockdown affects metabolism and insulin secretion

The effects of attenuated fission and reduced mitochondrial autophagy on mitochondrial respiratory function were assessed by measuring cellular oxygen consumption (Figure 8). An uncoupler, FCCP (5 μM) or DNP (100 μM), was added to collapse $\Delta\psi_m$ and assess maximal respiration capacity of the cell. It was found that the respiratory capacity of INS1 cells expressing *FIS1* RNAi or DRP1-DN was reduced by 48% ($n=4$) and 32% ($n=4$), respectively ($P<0.001$ in both the groups) (Figure 8A). Overexpression of RNAi-resistant *FIS1* together with *FIS1* RNAi ($n=3$) restored maximal respiration to the same level of INS1 cells expressing control RNAi ($n=3$, $P=0.72$).

To determine if a FIS1 knockdown affected mitochondrial protein synthesis, we measured the expression levels of the mtDNA-encoded subunit I of COX. We found that FIS1 knockdown for 10 days had no effect on subunit I expression (Figure 8B). The antiapoptotic effect of *FIS1* RNAi treatment was validated to exclude technical artifacts as a cause for the metabolic phenotype (Supplementary Figure S7).

To determine if a reduction in autophagy by itself can affect OXPHOS activity, oxygen consumption was monitored in INS1 cells, C2C12 cells and MEF cells, where autophagy was inhibited by two different mechanisms. Autophagy inhibition with 2 mM 3-MA over 5 days in INS1 cells reduced maximal respiration to ∼50% of the control condition ($P<0.001$, Figure 8A). ATG5 is an essential component for the assembly of the isolation membrane of the APs (Pyo *et al*, 2005). ATG5-deficient MEF cells had maximal respiration reduced by ∼40% (Figure 8A). Treatment of C2C12 mouse myoblasts cells with 3-MA (1 mM) resulted in a ∼16% reduction in maximal oxygen consumption ($P=0.04$).

The INS1 cells used here were derived from rat insulinoma (pancreatic tumor β-cells) and are characterized by a linear relationship between insulin secretion and glucose concentration within a range of 2–10 mM (Hohmeier *et al*, 2000). At basal glucose concentration (2 mM), there was no significant difference in insulin secretion between *FIS1* RNAi and the control RNAi cells ($n=5$, $P=0.57$; Figure 8C). Elevation of media glucose concentration to 8 mM increased insulin secretion in both cell types ($P<0.001$; Figure 8C). However, in *FIS1* RNAi the magnitude of glucose-stimulated insulin secretion (GSIS) was smaller than control RNAi cells ($n=5$, $P=0.02$).

Discussion

This study addresses the hypothesis that mitochondrial dynamics functions as a quality control mechanism that governs mitochondrial turnover. It demonstrates that fusion triggers fission and that fusion is a selective process, together resulting in a repetitive process that segregates less active mitochondria from the networking population. Inhibiting the occurrence of cycles of fusion and fission by *FIS1* RNAi or DRP1-DN resulted in the prevention of mitochondrial autophagy and the accumulation of damaged mitochondrial material, leading to decreased metabolic function and insulin secretion (Figure 9). The link between mitochondrial dynamics and autophagy is demonstrated both ways: on one hand fission is the event that produces depolarized mitochondria; reduced fission or increased fusion inhibit mitochondrial autophagy. On the other hand, mitochondria inside APs are found to have lost OPA1 and $\Delta\psi_m$ before being targeted by APs, two features, which would make them fusion incompetent.

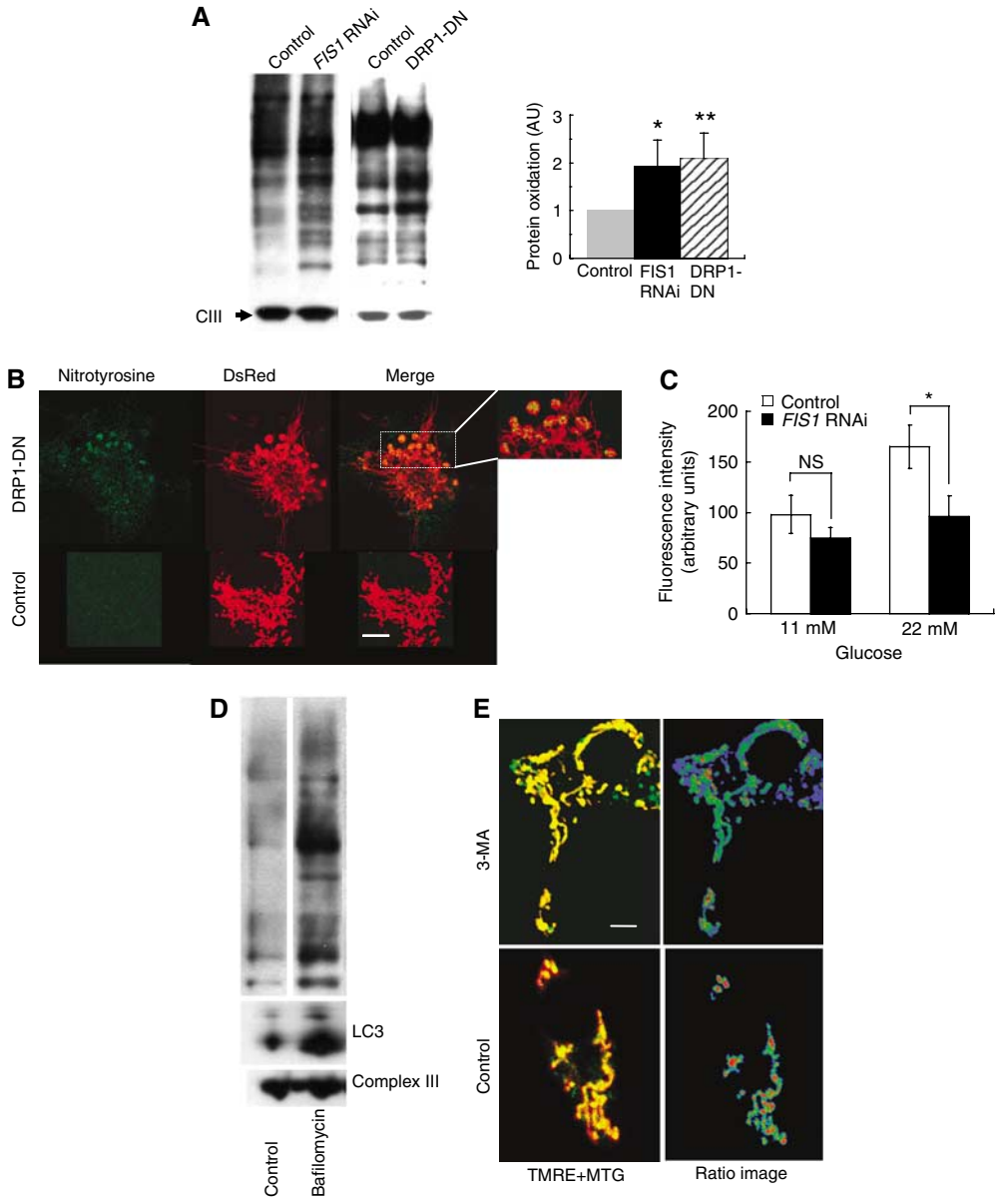

Figure 7 Inhibition of fission or autophagy results in increased protein oxidative damage. (**A**) Level of oxidized mitochondrial protein in mitochondria purified from *FIS1* RNAi ($n=3$), DRP1-DN ($n=4$) and their respective control cells. The blot detects carbonyl groups on amino-acid side chains (Oxiblot analysis, see Materials and methods). Loading control CIII, mitochondrial ComplexIII Core I (*$P<0.03$, **$P<0.04$). (**B**) COS7 cells coexpressing DRP1-DN and mtDsRed (red) were fixed, permeabilized and stained with a monoclonal antibody against nitrotyrosine (green). Control cells were infected with mtPA-GFP lentivirus. DRP1-DN cells show increased nitrotyrosine immunoreactivity in mitochondria, particularly in the distal and enlarged ends. Scale bar, 15 μm (see also Supplementary Figure S9). (**C**) Knockdown of FIS1 does not increase ROS production. ROS production in *FIS1* RNAi and control cells as measured by DHE FI under different glucose levels. Cells were loaded with dye and FI was measured before and 10 min after changing of glucose concentration (NS, non-significant; $P=0.5$; *$P<0.001$). (**D**) Inhibition of autophagy results in increased protein oxidative damage. Treatment of INS1 cells with bafilomycin (blocking autophagy by preventing fusion with lysosomes, 0.1 μM for 3 h) results in the accumulation of oxidized proteins in mitochondria, which is shown by increased level of carbonylated amino acids in isolated mitochondria. (**E**) Inhibition of autophagy generates $\Delta\psi_m$ heterogeneity. INS1 cells were treated with 3-MA (2 mM for 5 days) and then stained with TMRE and mitotracker green. Ratio image of red/green represents $\Delta\psi_m$ and is shown in pseudocolor where depolarized mitochondria appear blue. Note the increase in subcellular $\Delta\psi_m$ heterogeneity and the appearance of depolarized units with low TMRE (see also Supplementary Figure S4A–C). Scale bar, 5 μm.

Mitochondrial fusion is selective

Fusion was determined to be a selective process using two different approaches. First, a group of mitochondria was tagged by photoactivation of mtPA-GFP. A subpopulation was identified that did not exchange mtPA-GFP with unlabeled units (Figure 1). Second, daughters of mitochondrial fission were tracked and found to possess unequal probabilities of undergoing subsequent fusion (Figure 4). In both cases, a similar level of $\Delta\psi_m$ depolarization was identified in the non-fusing mitochondria.

While previous studies have demonstrated that uncoupling drugs cause overall mitochondrial fragmentation and arrest fusion (Legros *et al*, 2002; Ishihara *et al*, 2003; Meeusen *et al*, 2004; Malka *et al*, 2005), the relevance of these observations

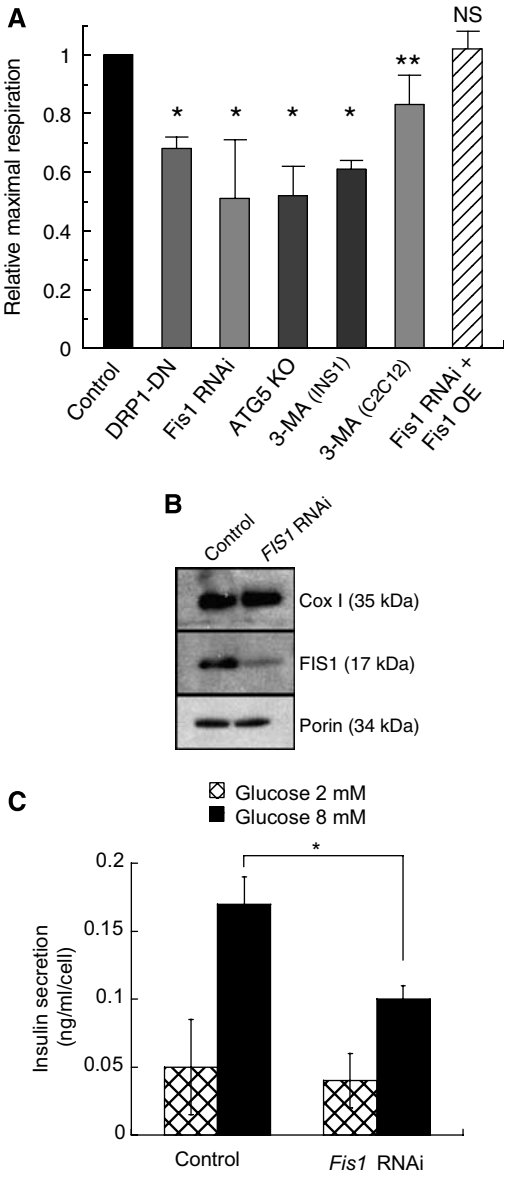

Figure 8 Altered metabolism accompanies decreased fission and autophagy. (**A**) FIS1 and DRP1 knockdown reduced maximal respiratory chain capacity in *FIS1* RNAi and DRP1-DN compared with their control ($n=4$ in each group; glucose = 11 mM). Inhibition of autophagy by 3-MA in INS1 cells (2 mM, 5 days, $n=4$) and C2C12 cells (1 mM, 5 days, $n=4$) showed significant decrease in respiratory capacity. ATG5-deficient MEF cells ($n=4$) had significantly decreased respiratory capacity compared with control MEF cells. Maximal respiration was tested using 5 μM FCCP or 100 μM DNP (*$P<0.001$, **$P<0.04$). (**B**) Expression of mtDNA-encoded subunit I of cytochrome oxidase (COX I) in INS1 cells infected with *FIS1* RNAi and control RNAi lentiviruses and tested after 1 week. (**C**) GSIS in *FIS1* RNAi and control RNAi cells ($n=5$ for each column, *$P<0.05$). Values are normalized to number of cells in each well and represent 30 min stimulation.

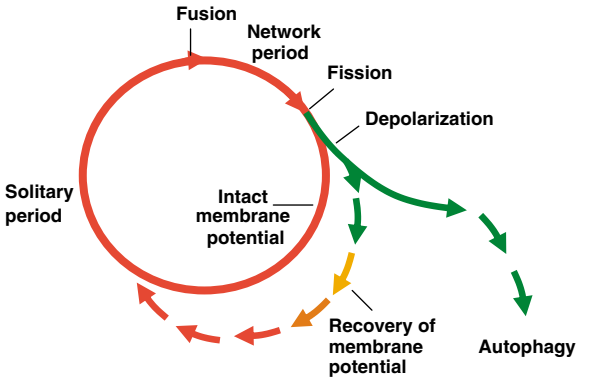

Figure 9 A model of the mitochondrion's life cycle that integrates mitochondrial dynamics and turnover. The mitochondrion cyclically shifts between a post fusion state (network) and a post fission state (solitary). Fusion is brief and triggers fission. Following a fission event, the daughter mitochondrion may either maintain intact membrane potential (red line) or depolarize (green line). If it depolarizes, it is unlikely to proceed to a subsequent fusion, unless it re-polarizes. After being depolarized and solitary for a few hours, the mitochondrion is removed by autophagy.

to fusion in the undisturbed cell has not been addressed. The present study is the first demonstration in living cells that mitochondrial fusion occurs preferentially between mitochondria with higher $\Delta\psi_m$, and generates an isolated subpopulation of non-fusing mitochondria. Moreover, these results demonstrate that a physiologically relevant reduction in $\Delta\psi_m$ impacts the prevalence of fusion. As each fusing mitochondrion requires intact $\Delta\psi_m$ to achieve matrix fusion, the process is unlikely to rescue dysfunctional units with altered $\Delta\psi_m$. Yet, the selectivity of the fusion process does not rule out the view that mitochondrial fusion serves as an inter-mitochondrial complementary route for metabolites and mtDNA between mitochondria with intact $\Delta\psi_m$ (Nakada *et al*, 2001).

Conversely, $\Delta\psi_m$ is influenced when fusion is inhibited (Olichon *et al*, 2003; Chen *et al*, 2005), suggesting that reduced fusion capacity could be either the cause or the result of $\Delta\psi_m$ depolarization. Experiments presented here conclude that depolarization occurs immediately subsequent to fission and not as a delayed consequence of reduced fusion capacity. The stability of $\Delta\psi_m$ of the individual mitochondria at all times other than the immediate post-fission period, as reported here, further supports the conclusion that reduced fusion over a period of an hour does not compromise the bioenergetic parameters of the individual unit.

OPA1 as a mechanism for selective fusion

In addition to having reduced $\Delta\psi_m$, non-fusing mitochondria were characterized by depletion in OPA1 immunoreactivity, providing a possible explanation for the reduced fusion capacity (Figure 5). Recently, a protonophore-induced complete collapse of $\Delta\psi_m$ of the entire cell mitochondria was shown to trigger proteolytic cleavage or degradation of OPA1 long (l-)isoforms (Griparic *et al*, 2004; Duvezin-Caubet *et al*, 2006; Ishihara *et al*, 2006; Song *et al*, 2007). Here we show that minute and physiological depolarization of the individual mitochondrion in the context of the intact cell is accompanied by reduced OPA1 levels and diminished fusion capacity. These results further emphasize that depletion of OPA1 in the individual mitochondrion within the intact cell may preclude fusion and metabolic complementation even if surrounded by fusion-competent mitochondria (Figure 1). The dependency of OPA1 proteolysis on ATP concentration may explain how small changes in $\Delta\psi_m$ may lead to such profound reduction in fusion capacity (Herlan *et al*, 2004).

Given that a depolarization of 14 mV can drop ATP synthesis by up to 10-fold (Nicholls, 2004), a depolarization of ~7 mV, as found in the non-fusing mitochondria, may alter fusion through ATP depletion or processing of OPA1.

The attenuated OPA1 staining seen in non-fusing mitochondria in this study reflects mainly the degradation of OPA1 and not their proteolytic cleavage, since the antibody used here targeted the common region for the l- and s-isoforms. This finding is in accordance with Song *et al* (2007) showing that complete degradation (rather than proteolytic cleavage) is the principal route of processing of the long isoforms (splice 1 and 2) of OPA1, and is therefore likely to be an underestimation of the actual depletion in OPA1 long isoforms.

Metabolic consequences of single fission events

We found that mitochondrial fission results in predictive and asymmetric changes in $\Delta\psi_m$ of the two daughters (Figures 2 and 3). This is the first measurement of a metabolic consequence of single fission event. It demonstrates for the first time that although the mitochondrial network permits diffusion and equilibration of matrix and membrane components, fission results in the separation of metabolically uneven daughters. The asymmetrical nature of the fission event may have a role in directing different segments of the mitochondrial network to disparate fates and in endowing a functional specificity to a sorting mechanism of any kind.

A number of potential mechanisms underlying the uneven $\Delta\psi_m$ of the daughter mitochondria were ruled out, including PTP opening, disruption of membrane integrity and increased ATP synthase activity. Although the mechanism is yet to be resolved, EM studies of cells treated with agents that impose immediate and extensive mitochondrial fragmentation observed neighboring fragments with disparate cristae structures, suggesting the possibility that fission of mitochondria might yield daughters with unequal membranous structures (Barsoum *et al*, 2006).

Is autophagy preventing subsequent fusion of the depolarized daughter unit?

The reduced probability of depolarized mitochondria to proceed into a consecutive fusion raised the possibility that fusion is prevented by an isolation membrane of forming APs.

Our observations indicate that in the absence of a stress-related death signal, mitochondria depolarize hours before being engulfed by the isolation membrane of the APs (Figure 4). These suggest that autophagy does not contribute to the observed depolarization of the daughter unit or its segregation from the fusing population. The time interval between mitochondrial depolarization and colocalization with lysosomes was reported to be ~20 min (Elmore *et al*, 2001). However, the time gap estimated by Elmore and coworkers was measured under autophagy inducers (starvation and glucagon) and by the detection of lysosomal rather than AP isolation membrane markers.

The decreased OPA1 immunoreactivity in mitochondria that have been targeted by autophagy and in non-fusing mitochondria (Figure 5) provides a potential link between depolarization, reduced fusion capacity and removal by autophagy. The ability of OPA1 overexpression to reduce mitochondrial autophagy indicates that OPA1 plays a role in determining the fate of mitochondria. This may be direct, by preventing AP targeting, or indirect, by either increasing bioenergetic efficiency or increasing the mitochondrial fusion probability, leading to a more homogenous network and reduced chance for the generation of depolarized mitochondria.

Mitochondrial fission is essential for autophagy

This study and others have demonstrated that depolarized mitochondria are targeted by autophagy. We showed here that the main source of depolarized mitochondria is the fission event. Together, these observations raise the possibility that fission might be essential for mitochondrial autophagy.

Indeed, inhibition of fission resulted in the inhibition of mitochondrial, but not ER, autophagy (Figure 6). Formation of APs, lysosomes mass, generation of the autophagolysosomes and digestion of their content were not affected. We conclude that mitochondrial autophagy is inhibited before assembly of the isolation membrane, and implicate mitochondrial fission as a mediator of mitochondrial turnover. However, the role fission play is in reducing mitochondrial size may only be permissive and is unlikely to function as a trigger for autophagy, since overexpression of OPA1, which we found to inhibit mitochondrial autophagy, is accompanied by segmentation of the mitochondrial network, as reported by others and observed here in INS1 cells (Griparic *et al*, 2004; Chen *et al*, 2005).

In summary, mitochondrial fission is the occasional producer of daughter mitochondria that are characterized by three features found in autophagocytosed mitochondria: reduced $\Delta\psi_m$, decreased OPA1 and reduced size. Before being targeted by autophagy, these mitochondria have reduced fusion capacity and are less likely to be recruited by fusion into a polarized network (Figure 9).

Mitochondrial dynamics and insulin secretion

Defective GSIS observed in diabetic models has been strongly associated with mitochondrial dysfunction and specifically with abnormal respiratory chain activity (Maechler *et al*, 1999; Lowell and Shulman, 2005). Inhibition of fission reduced maximal respiratory chain capacity, an observation that could explain the suppression of GSIS (Figure 8) as well as the reduction in ROS production in the *FIS1* RNAi cells.

The accumulation of oxidized mitochondrial protein in the absence of increased ROS in *FIS1* RNAi cells suggests that inhibition of fission results in reduced mitochondrial turnover (Figure 7). This is in line with experiments in which removal of mitochondria by autophagy was arrested, leading to a comparable decrease in respiratory chain activity. ATG5−/− fibroblasts and cells treated with the autophagy inhibitor 3-MA, two mechanistically distinct cellular models for autophagy inhibition, were found to have reduced respiratory capacity, similar to *FIS1* RNAi and DRP1-DN-treated cells. This agrees with studies on fibroblasts in which inhibition of autophagy by 3-MA or by targeting of *ATG7* resulted in the accumulation of mitochondria with lowered $\Delta\psi_m$ in the former and in alteration of mitochondrial morphology in the latter (Stroikin *et al*, 2004; Komatsu *et al*, 2005). However, additional studies will be required to determine what is the isolated contribution of the *FIS1* RNAi and DRP1-DN-induced

inhibition of autophagy to the accumulation of damaged mitochondrial proteins and mitochondrial dysfunction.

The combination of fission, selective fusion and autophagy described here may represent a quality control mechanism of the mitochondrial population (Figure 9). Why this mechanism fails to select against dysfunctional units or promotes respiratory compromised mitochondria under certain circumstances remains unclear. A defect in the quality control mechanism would lead to a progressive, diverse and insult-dependent decrease in function such as found in metabolic diseases and aging. In this context, the quality control checkpoint presented here may provide a potential mechanism for the induced senescence observed in cells in which fission has been hampered (Yoon *et al*, 2006; Lee *et al*, 2007).

Materials and methods

Animals
Twelve-week-old male C57BL6 mice were used.

Islet isolation, primary cells and cell line culture
Islets were isolated, dispersed and plated as previously described (Heart *et al*, 2006).

Cell lines
ATG5+/+ and ATG5−/− mouse embryonic fibroblasts (MEFs) transfected with pEF321-T, and an SV40 large T antigen expression vector were a generous gift from N Mizushima and were previously described (Kuma *et al*, 2004).

DNA plasmids, constructs
Construction of viruses delivering mtPA-GFP, DRP1-DN, pWPI, *FIS1* shRNA, control shRNA, LC3:GFP, mtDsRed and OPA1 OE is described in detail in the Supplementary data.

Confocal microscopy
Confocal microscopy was performed using a Zeiss LSM 510 Meta microscope. Detailed description of imaging protocols and controls for imaging artifacts is found in the Supplementary data.

Measurement of ROS production
Cells were loaded with 1 μM DHE (Invitrogen, Carlsbad, CA, USA) for 20 min at 37°C. Images were analyzed Using Metamorph imaging software (Molecular Devices, Sunnyvale, CA, USA).

O_2 consumption
Oxygen consumption in INS1 (expressing DRP1-DN) and in C2C12 cells was measured by an XF24 bioenergetic assay (Seahorse Bioscience, Billerica, MA, USA). Assays have been previously described in detail (Wu *et al*, 2007) and explained in the Supplementary data.

Oxygen consumption in INS1 (expressing *FIS1* RNAi) and in ATG5 MEF null cells was measured as previously described (Corkey *et al*, 1986) (see Supplementary data).

Immunostaining
Cells were fixed with 4% paraformaldehyde for 15 min, washed, permeabilized in 0.5% Triton-X for 15 min, washed, blocked with 1% BSA/PBS for 15 min, incubated with primary antibody for 1 h, washed, incubated with the secondary antibody for 1 h, and washed and mounted with mowiol mounting media. All washes were with PBS and all procedures were performed at room temperature. The following primary antibodies were used: OPA1 (BD, USA, cat no. 612606; 1:100) and anti-nitrotyrosine (Upstate, MA; 1:500). Secondary antibodies were from Zymed (Invitrogen, Carlsbad, CA).

Insulin secretion from INS-1 cells
The above procedure was performed as previously described (Noel *et al*, 1997) (see also Supplementary data).

Protein oxidation detection
Mitochondrial isolation was performed using a mitochondrial isolation kit (Pierce, cat no. 89801), followed by using the Oxyblot™ protein oxidation detection kit (Chemicon International) (see Supplementary data).

Statistics
Unless stated otherwise error bars indicate SD and unpaired *t*-test was used to validate statistical differences.

Supplementary data
Supplementary data are available at *The EMBO Journal* Online (http://www.embojournal.org).

Acknowledgements

This work was supported by National Institutes of Health Grants 5R01HL071629-03, and R01 DK074778 and P41 RR001395, and by NSF grant DBI-0215829. We thank Solomon Graf, Israel Biran, Dani Dagan, Roland Lill, David Nicholls, Eric Schon, Gyorgy Hajnoczki, Gordon Yaney, Keith Tornheim, Nika Danial and Channing Yu for helpful discussions. We thank Peter Smith and Louis Kerr at the MBL and Craig Lassy at Zeiss for supporting the confocal microscopy studies.

References

Alavi MV, Bette S, Schimpf S, Schuettauf F, Schraermeyer U, Wehrl HF, Ruttiger L, Beck SC, Tonagel F, Pichler BJ, Knipper M, Peters T, Laufs J, Wissinger B (2007) A splice site mutation in the murine Opa1 gene features pathology of autosomal dominant optic atrophy. *Brain* **130:** 1029–1042

Arimura S, Yamamoto J, Aida GP, Nakazono M, Tsutsumi N (2004) Frequent fusion and fission of plant mitochondria with unequal nucleoid distribution. *Proc Natl Acad Sci USA* **101:** 7805–7808

Barsoum MJ, Yuan H, Gerencser AA, Liot G, Kushnareva Y, Graber S, Kovacs I, Lee WD, Waggoner J, Cui J, White AD, Bossy B, Martinou JC, Youle RJ, Lipton SA, Ellisman MH, Perkins GA, Bossy-Wetzel E (2006) Nitric oxide-induced mitochondrial fission is regulated by dynamin-related GTPases in neurons. *EMBO J* **25:** 3900–3911

Chan DC (2006) Mitochondria: dynamic organelles in disease, aging, and development. *Cell* **125:** 1241–1252

Chen H, Chomyn A, Chan DC (2005) Disruption of fusion results in mitochondrial heterogeneity and dysfunction. *J Biol Chem* **280:** 26185–26192

Cipolat S, Martins de Brito O, Dal Zilio B, Scorrano L (2004) OPA1 requires mitofusin 1 to promote mitochondrial fusion. *Proc Natl Acad Sci USA* **101:** 15927–15932

Corkey BE, Duszynski J, Rich TL, Matschinsky B, Williamson JR (1986) Regulation of free and bound magnesium in rat hepatocytes and isolated mitochondria. *J Biol Chem* **261:** 2567–2574

Duvezin-Caubet S, Jagasia R, Wagener J, Hofmann S, Trifunovic A, Hansson A, Chomyn A, Bauer MF, Attardi G, Larsson NG, Neupert W, Reichert AS (2006) Proteolytic processing of OPA1 links mitochondrial dysfunction to alterations in mitochondrial morphology. *J Biol Chem* **281:** 37972–37979

Elmore SP, Qian T, Grissom SF, Lemasters JJ (2001) The mitochondrial permeability transition initiates autophagy in rat hepatocytes. *FASEB J* **15:** 2286–2287

Griparic L, van der Wel NN, Orozco IJ, Peters PJ, van der Bliek AM (2004) Loss of the intermembrane space protein Mgm1/OPA1 induces swelling and localized constrictions along the lengths of mitochondria. *J Biol Chem* **279:** 18792–18798

Heart E, Corkey RF, Wikstrom JD, Shirihai OS, Corkey BE (2006) Glucose-dependent increase in mitochondrial membrane potential, but not cytoplasmic calcium, correlates with insulin secretion in single islet cells. *Am J Physiol Endocrinol Metab* **290:** E143–E148

Herlan M, Bornhovd C, Hell K, Neupert W, Reichert AS (2004) Alternative topogenesis of Mgm1 and mitochondrial morphology

depend on ATP and a functional import motor. *J Cell Biol* **165:** 167–173

Hohmeier HE, Mulder H, Chen G, Henkel-Rieger R, Prentki M, Newgard CB (2000) Isolation of INS-1-derived cell lines with robust ATP-sensitive K+ channel-dependent and -independent glucose-stimulated insulin secretion. *Diabetes* **49:** 424–430

Ishihara N, Fujita Y, Oka T, Mihara K (2006) Regulation of mitochondrial morphology through proteolytic cleavage of OPA1. *EMBO J* **25:** 2966–2977

Ishihara N, Jofuku A, Eura Y, Mihara K (2003) Regulation of mitochondrial morphology by membrane potential, and DRP1-dependent division and FZO1dependent fusion reaction in mammalian cells. *Biochem Biophys Res Commun* **301:** 891–898

Komatsu M, Waguri S, Ueno T, Iwata J, Murata S, Tanida I, Ezaki J, Mizushima N, Ohsumi Y, Uchiyama Y, Kominami E, Tanaka K, Chiba T (2005) Impairment of starvation-induced and constitutive autophagy in Atg7-deficient mice. *J Cell Biol* **169:** 425–434

Kuma A, Hatano M, Matsui M, Yamamoto A, Nakaya H, Yoshimori T, Ohsumi Y, Tokuhisa T, Mizushima N (2004) The role of autophagy during the early neonatal starvation period. *Nature* **432:** 1032–1036

Lee S, Jeong SY, Lim WC, Kim S, Park YY, Sun X, Youle RJ, Cho H (2007) Mitochondrial fission and fusion mediators, hFis1 and OPA1, modulate cellular senescence. *J Biol Chem* **282:** 22977–22983

Legros F, Lombes A, Frachon P, Rojo M (2002) Mitochondrial fusion in human cells is efficient, requires the inner membrane potential, and is mediated by mitofusins. *Mol Biol Cell* **13:** 4343–4354

Levine B, Yuan J (2005) Autophagy in cell death: an innocent convict? *J Clin Invest* **115:** 2679–2688

Lowell BB, Shulman GI (2005) Mitochondrial dysfunction and type 2 diabetes. *Science* **307:** 384–387

Maechler P, Jornot L, Wollheim CB (1999) Hydrogen peroxide alters mitochondrial activation and insulin secretion in pancreatic beta cells. *J Biol Chem* **274:** 27905–27913

Malka F, Guillery O, Cifuentes-Diaz C, Guillou E, Belenguer P, Lombes A, Rojo M (2005) Separate fusion of outer and inner mitochondrial membranes. *EMBO Rep* **6:** 853–859

Meeusen S, McCaffery JM, Nunnari J (2004) Mitochondrial fusion intermediates revealed *in vitro*. *Science* **305:** 1747–1752

Nakada K, Inoue K, Ono T, Isobe K, Ogura A, Goto YI, Nonaka I, Hayashi JI (2001) Inter-mitochondrial complementation: mitochondria-specific system preventing mice from expression of disease phenotypes by mutant mtDNA. *Nat Med* **7:** 934–940

Nicholls DG (2004) Mitochondrial membrane potential and aging. *Aging Cell* **3:** 35–40

Noel RJ, Antinozzi PA, McGarry JD, Newgard CB (1997) Engineering of glycerol-stimulated insulin secretion in islet beta cells. Differential metabolic fates of glucose and glycerol provide insight into mechanisms of stimulus–secretion coupling. *J Biol Chem* **272:** 18621–18627

Okamoto K, Shaw JM (2005) Mitochondrial morphology and dynamics in yeast and multicellular eukaryotes. *Annu Rev Genet* **39:** 503–536

Olichon A, Baricault L, Gas N, Guillou E, Valette A, Belenguer P, Lenaers G (2003) Loss of OPA1 perturbates the mitochondrial inner membrane structure and integrity, leading to cytochrome *c* release and apoptosis. *J Biol Chem* **278:** 7743–7746

Priault M, Salin B, Schaeffer J, Vallette FM, di Rago JP, Martinou JC (2005) Impairing the bioenergetic status and the biogenesis of mitochondria triggers mitophagy in yeast. *Cell Death Differ* **12:** 1613–1621

Pyo JO, Jang MH, Kwon YK, Lee HJ, Jun JI, Woo HN, Cho DH, Choi B, Lee H, Kim JH, Mizushima N, Oshumi Y, Jung YK (2005) Essential roles of Atg5 and FADD in autophagic cell death: dissection of autophagic cell death into vacuole formation and cell death. *J Biol Chem* **280:** 20722–20729

Skulachev VP (2001) Mitochondrial filaments and clusters as intracellular power-transmitting cables. *Trends Biochem Sci* **26:** 23–29

Song Z, Chen H, Fiket M, Alexander C, Chan DC (2007) OPA1 processing controls mitochondrial fusion and is regulated by mRNA splicing, membrane potential, and Yme1L. *J Cell Biol* **178:** 749–755

Stojanovski D, Koutsopoulos OS, Okamoto K, Ryan MT (2004) Levels of human Fis1 at the mitochondrial outer membrane regulate mitochondrial morphology. *J Cell Sci* **117:** 1201–1210

Stroikin Y, Dalen H, Loof S, Terman A (2004) Inhibition of autophagy with 3-methyladenine results in impaired turnover of lysosomes and accumulation of lipofuscin-like material. *Eur J Cell Biol* **83:** 583–590

Twig G, Graf SA, Wikstrom JD, Mohamed H, Haigh SE, Elorza A, Deutsch M, Zurgil N, Reynolds N, Shirihai OS (2006) Tagging and tracking individual networks within a complex mitochondrial web with photoactivatable GFP. *Am J Physiol Cell Physiol* **291:** C176–C184

Wu M, Neilson A, Swift AL, Moran R, Tamagnine J, Parslow D, Armistead S, Lemire K, Orrell J, Teich J, Chomicz S, Ferrick DA (2007) Multiparameter metabolic analysis reveals a close link between attenuated mitochondrial bioenergetic function and enhanced glycolysis dependency in human tumor cells. *Am J Physiol Cell Physiol* **292:** C125–C136

Yoon Y, Krueger EW, Oswald BJ, McNiven MA (2003) The mitochondrial protein hFis1 regulates mitochondrial fission in mammalian cells through an interaction with the dynamin-like protein DLP1. *Mol Cell Biol* **23:** 5409–5420

Yoon YS, Yoon DS, Lim IK, Yoon SH, Chung HY, Rojo M, Malka F, Jou MJ, Martinou JC, Yoon G (2006) Formation of elongated giant mitochondria in DFO-induced cellular senescence: involvement of enhanced fusion process through modulation of Fis1. *J Cell Physiol* **209:** 468–480

